01 May 2022

Use of Saturated Lightweight Sand to Improve the Mechanical and Microstructural Properties of UHPC with Fiber Alignment

Huanghuang Huang

Le Teng

Xiaojian Gao

Kamal Khayat
Missouri University of Science and Technology, khayatk@mst.edu

et. al. For a complete list of authors, see https://scholarsmine.mst.edu/civarc_enveng_facwork/2322

Recommended Citation

H. Huang et al., "Use of Saturated Lightweight Sand to Improve the Mechanical and Microstructural Properties of UHPC with Fiber Alignment," *Cement and Concrete Composites*, vol. 129, article no. 104513, Elsevier, May 2022.
The definitive version is available at https://doi.org/10.1016/j.cemconcomp.2022.104513

Cement and Concrete Composites 129 (2022) 104513

Contents lists available at ScienceDirect

Cement and Concrete Composites

journal homepage: www.elsevier.com/locate/cemconcomp

Use of saturated lightweight sand to improve the mechanical and microstructural properties of UHPC with fiber alignment

Huanghuang Huang [a,b,c], Le Teng [d], Xiaojian Gao [b,**], Kamal H. Khayat [d,*], Fazhou Wang [a,c], Zhichao Liu [a,c]

[a] School of Materials Science and Engineering, Wuhan University of Technology, Wuhan, 430070, China
[b] School of Civil Engineering, Harbin Institute of Technology, Harbin, 150090, China
[c] State Key Laboratory of Silicate Materials for Architectures, Wuhan University of Technology, Wuhan, 430070, China
[d] Department of Civil, Architectural and Environmental Engineering, Missouri University of Science and Technology, Rolla, MO, 65401, USA

ARTICLE INFO

Keywords:
Fiber alignment
Lightweight sand
Microstructure
Mechanical properties
UHPC

ABSTRACT

This paper studied the influence of pre-saturated lightweight sand (LWS) on the mechanical and microstructural properties of UHPC cast with steel fiber alignment. The changes in hydration kinetics, porosity, nano-mechanical, and mechanical properties were studied. The LWS was used at 0–50% replacement volumes of total sand. Predominant fiber alignment was favored through a flow-induced casting method during casting of flexural prisms. Experiment results showed that the 28-d autogenous shrinkage was decreased from 450 to 275 μm/m with the LWS content increasing from 0 to 50%. The addition of 20% LWS led to maximum increases of 15%, 15%, and 20% in compressive strength, flexural strength, and T150, respectively, relative to UHPC made without any LWS. The use of 20% LWS combined with fiber alignment led to a synergistic effect of 45% and 40% on enhancing the flexural strength and T150, respectively, relative to UHPC without LWS and having random fiber orientation. The addition of LWS can enhance the cement hydration given the internal curing effect. Such enhanced cement hydration increased the percentage of high density and ultra-high density C–S–H from 50% to 75% and reduced the 28-d porosity from 12.5% to 9.5% with the use of 20% LWS. On the other hand, such internal curing can be overwhelmed by the introduced pores of LWS when excessive LWS was used, which led to significant increase in porosity of UHPC.

1. Introduction

Ultra-high performance concrete (UHPC) has been regarded as one of the most innovative building materials in the past three decades, given its significantly great mechanical properties and durability [1–3]. Such superior performance makes it a great construction material in large-span bridges and buildings as well as repair applications [4,5]. Generally, UHPC is designed with high packing density of binder and aggregate materials and a low water-to-binder ratio to secure a low porosity of the material [6–8]. Steel fibers are added to enhance mechanical properties and ductility [9,10]. The crack-bridging capacity of fibers is highly dependent on their orientation, which can be maximized by rheology adjustment of UHPC mortar [11–13] and optimization of the casting method [14–16].

However, UHPC can exhibit high degree of self-desiccation that can result in high autogenous shrinkage, which is mainly attributed to the low water-to-binder ratio [17,18]. This can increase the risk of cracking, particularly in presence of restraint [19]. Such cracking can reduce mechanical properties and durability, bond strength for overlay applications, and reduction of structural integrity [20,21].

Several methods, including the use of a shrinkage-reducing, expansive, and internal curing agents were reported to reduce the shrinkage of cement-based materials [22–28]. The internal curing agent includes the superabsorbent polymer (SAP) and lightweight aggregate (LWA). The SAP and LWA with high porosity can absorb a large amount of water and release it over time with the decrease of internal humidity of the cement matrix [29,30]. This can therefore compensate for some of the loss of internal humidity during cement hydration and secure internal curing of the cement matrix. On the other hand, the use of coarse aggregate can reduce the autogenous shrinkage of UHPC given its restraining effect

* Corresponding author.
** Corresponding author.
E-mail addresses: gaoxj@hit.edu.cn (X. Gao), khayatk@mst.edu (K.H. Khayat).

https://doi.org/10.1016/j.cemconcomp.2022.104513
Received 8 December 2021; Received in revised form 1 March 2022; Accepted 25 March 2022
Available online 28 March 2022

Table 1
Material properties of binders and sands.

	Cement	SF	FAC	RS	MS	LWS
CaO (%)	64.50	0.40	28.10	1.72	9.42	3.40
SiO_2 (%)	19.72	95.50	36.50	80.30	86.50	57.60
Al_2O_3 (%)	5.10	0.70	24.80	10.50	0.39	19.40
Fe_2O_3 (%)	2.76	0.30	5.20	3.43	1.47	9.60
MgO (%)	2.30	0.50	5.00	1.70	–	2.60
Na_2O eq. (%)	0.33	0.40	–	–	–	5.60
SO_3	3.25	–	2.50	1.07	–	0.60
Loss of ignition (%)	1.50	2.00	0.50	1.28	0.24	–
Apparent density (kg/m^3)	3150	2200	2700	2650	2640	1810
Blaine surface area (m^2/kg)	562	–	465	–	–	–
B.E.T. (m^2/g)	–	18.2	–	–	–	–

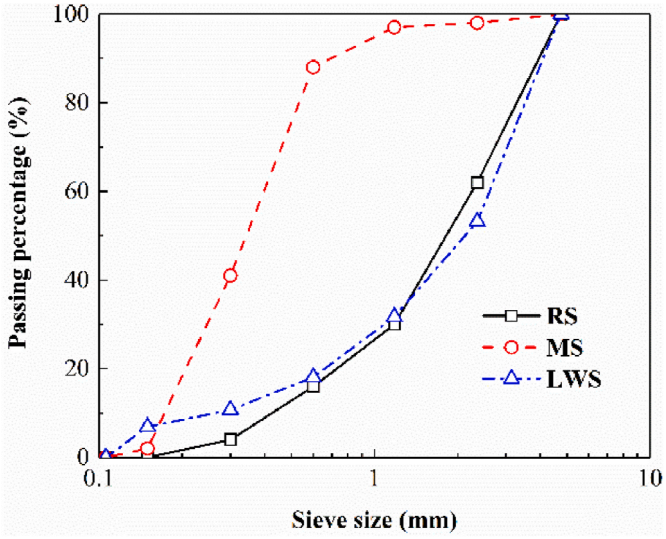

Fig. 1. Sieve analysis of three sands.

Table 2
Mixture proportions of UHPC containing various LWS contents.

Notation	Cement (kg/m^3)	FAC (kg/m^3)	SF (kg/m^3)	MS (kg/m^3)	RS (kg/m^3)	LWS (kg/m^3)	Steel fibers (% by volume of mixture)
Ref	650	405	41	300	704	0	2
LWS10					633	48	
LWS20					562	96	
LWS30					492	143	
LWS40					422	191	
LWS50					351	239	

[31]. For example, the autogenous shrinkage was decreased by 40% for UHPC containing coarse aggregate compared to that made without coarse aggregate [32]. However, the addition of coarse aggregate in UHPC can result in the decrease in mechanical properties given the greater interfacial transition zone.

The use of LWA in the UHPC made with conventional concrete sand is shown to enhance the mechanical performance of UHPC [21,33–35]. For example, the use of 25% lightweight sand (LWS) to replace river sand resulted in 135 μm/m decrease in autogenous shrinkage, 28 MPa increase in compressive strength, and 3 MPa enhancement in flexural strength of UHPC relative to UHPC without LWS addition. Further increase in LWS content to 75% reduced the compressive and flexural strengths by 30 and 15 MPa, respectively [33].

Despite significant enhancement of LWS on the performance of UHPC, the underlying enhancing mechanism of LWS, especially the effect of LWS on microstructure of cement matrix in the vicinity of the LWS (referred to here as the surrounding matrix) is not fully understood. The combined use of the LWS and fiber alignment can lead to a synergistic reinforcement effect on mechanical properties. However, such synergy effect has not been investigated before.

The objective of this paper was to investigate the influence of saturated LWS on mechanical and microstructural characteristics of UHPC cast with alignment of fibers in flexural specimens. The hydration kinetics, porosity, nano-mechanical characteristics, and mechanical properties of UHPC made with various LWS contents were studied. Moreover, the combined effect of internal curing of LWS and fiber alignment during the casting of UHPC flexural specimens on flexural properties is evaluated. LWS was used at 0–50% replacement volumes of total sand. Predominant fiber alignment was favored through a flow-induced casting method in preparing flexural samples.

2. Experimental program

2.1. Raw materials and mixture proportion

Binder materials, including Type III Portland cement, Class C fly ash (FAC), and silica fume (SF), were employed at volume ratios of 55%, 40%, and 5%, respectively. Three sands, including river sand (RS), masonry sand (MS), and lightweight sand (LWS), were employed. The material properties of binders and sands are summarized in Table 1.

The LWS was bought from the Northeast Solite located at Shepardsville in Kentucky. The 24-h and 72-h water absorption of LWS were 17.6% and 18.4%, respectively. The relative desorption of LWS tested using the centrifuge method and nominal maximum size were 96.4% and 4.75 mm. The sieve analysis of three sands is given in Fig. 1. The LWS was shown to have a similar particle size distribution compared to that of river sand. Therefore, the LWS was used to replace RS by volume in this study. The volume ratios of (RS + LWS) and MS were 70% and 30%, respectively, to secure a dense packing of solid raw materials [33]. Micro steel fibers (diameter: 0.2 mm, length: 13 mm) were utilized at 2%, by volume.

The polycarboxylate-based high-range water-reducer (HRWR) was employed at 0.42%, by mass of binder to ensure a self-consolidating performance of fresh mixture. Welan gum powder (WG) was used at 0.18%, by mass of binder to increase the viscosity of mixture to secure uniform dispersion of fiber and LWS [13]. The air-detraining admixture (ADA) was used at 0.4‰, by mass of binder to decrease the air content of mixture during mixing.

Table 2 summarizes the mixture proportions of UHPC containing various LWS contents. The *w/b* was fixed at 0.2. The LWS contents were investigated at 0, 10%, 20%, 30%, 40%, and 50% replacement volumes of the RS. These UHPC mixtures are referred to as Ref, LWS10, LWS20, LWS30, LWS40, and LWS50, respectively. The investigated mixture made without LWS corresponded to non-proprietary UHPC that has a target compressive strength of 120 MPa without heat or steam curing. This mixture met the ASTM C1856 and is proportioned as a cost-effective UHPC with the addition of large content of fly ash and ordinary sand [36].

2.2. Sample preparation

WG powder and 90% of the HRWR were premixed at 15 rps for 10 min to disperse the WG in the HRWR. UHPC mixtures were prepared as the following procedures: (1) binders and sands including LWS were mixed at 60 rpm for 2 min; (2) the pre-dispersed WG suspension, ADA, and 90% of mixing water were incorporated and mixed at 120 rpm for 3 min; and (3) the remainder of water and HRWR were incorporated and mixed at 120 rpm for 3 min (4) For preparing non-fibrous UHPC mortar, the mixing was remained for additional 4 min. For the preparation of UHPC containing 2% steel fibers, the fibers were incorporated in 1 min.

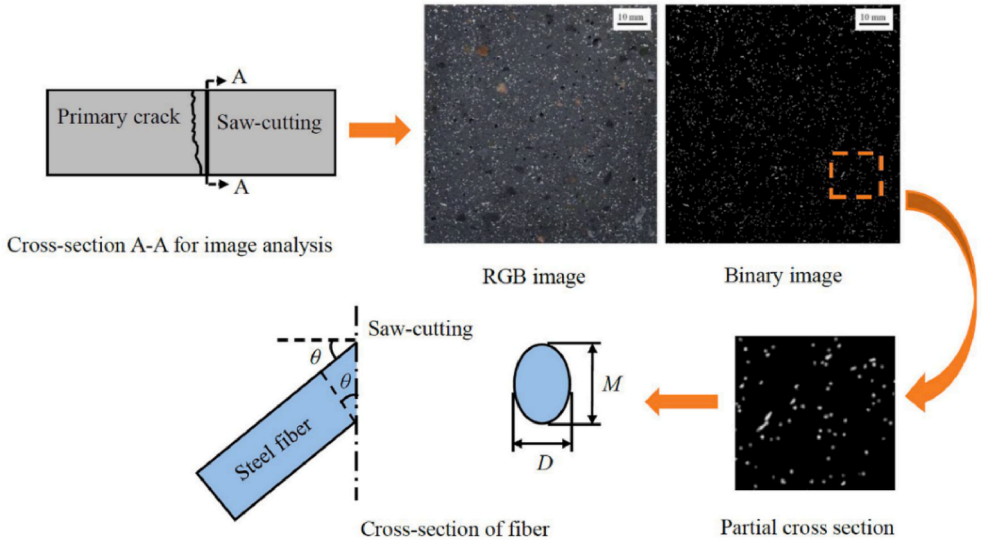

Fig. 2. Image analysis method for determination of fiber orientation.

The mixing was resumed at 120 rpm for 3 min to achieve a uniform fiber dispersion. It is important to note small part of the water close to the surface of LWS can break away during dry mixing. However, the LWS can easily absorb the water back after adding mixing water [28]. Therefore, the water absorbed in the pores of LWS was not influenced during mixture preparation.

The flow-induced casting method was employed to facilitate the alignment of fibers in the longitudinal direction of the beam samples [37,38]. Fresh mixture was cast through a L-shape device to facilitate flow into the mold through a 10-mm high outlet [37,38]. For the preparation of samples having random orientation, fresh mixture was cast from the middle of mold in one lift allowing the UHPC to flow into place [37]. This referred to the conventional method. The samples were cured with mold for 1 day at room with covering of plastic film. The samples were then cured in lime-saturated water at 21 ± 2 °C until testing age.

2.3. Testing methods

2.3.1. Fluidity and rheology of non-fibrous UHPC mortar

The mini-slump flow of non-fibrous mortar mixture was tested on the basis of ASTM C230/C230 M. The rheological properties (i.e., yield stress and plastic viscosity) of mixture were determined using a ConTec 5 rheometer. The testing procedure of rheological parameters was given in Ref. [11].

2.3.2. Hydration kinetics

The hydration kinetics of non-fibrous UHPC mortars containing various LWS contents were tested through a Calmetrix I-CAL 8000. Approximately 75 g mixture was used for the heat flow and cumulative heat test immediately after mixing. The mixture was sealed in a plastic bottle during testing and was tested for 48 h at temperature of 20 ± 0.1 °C.

2.3.3. Autogenous shrinkage

The autogenous shrinkage of non-fibrous UHPC mortar was tested according to ASTM C1698. Fresh mixture was cast and sealed in corrugated plastic tubes that was maintained at 23 ± 1 °C and RH of 50% ± 1%. The measurement started at the final setting of mixtures. The shrinkage values were tested daily in the first week and weekly until 28 d.

2.3.4. Mechanical properties

For each mixture, the compressive strength was evaluated based on three cubes measuring 50 mm in length in line with ASTM C109. The loading rate was set as 1.8 kN/min. The flexural strength was tested by four-point bending based on three beams measuring 76 × 76 × 406 mm ($b \times h \times l$) (ASTM C1609). The span and loading rate were 305 mm and 0.1 mm/min, respectively. The flexural strength (σ_f) is determined as:

$$\sigma_f = \frac{F_{max}L}{bh^2} \quad (1)$$

where F_{max} (N) is the maximum flexural load, and L (mm) is the span of the beam samples. The dissipated energy (T150) is expressed as the area under the flexural curve where the deflection value increases from 0 to $L/150$. The T150 can be applied to assess the toughness of UHPC. A greater toughness represents a greater crack-bridging effect of steel fibers, which is closely related to the interfacial performance between fiber and matrix. There is a concern that the internal curing of LWS can enhance the fiber-matrix interface, resulting in a higher toughness of UHPC [39].

2.3.5. Fiber orientation evaluation

After flexural testing, saw-cut sample near the dominant crack was used to determine the fiber orientation using image analysis method. The surface of saw-cut sample measuring 76 × 76 × 5 mm was sequentially ground using 80-, 180-, 400-, and 600-grit sand papers to improve the contrast between fibers and matrix. The surface was then photographed using a high-resolution camera to secure the pixels of 23,005 × 23,005. The achieved RGB image was converted to binary image to separate fibers from the matrix, as illustrated in Fig. 2.

For a single fiber embedded in the matrix, the fiber orientation angle (θ) is calculated as the ratio of minor axis (D) to major axis (M) determined from the fiber image, as given in Eq. (2):

$$\theta = arccos\left(\frac{D}{M}\right) \quad (2)$$

The fiber orientation coefficient (η_θ) in the longitudinal direction of beam samples is determined as [40]:

$$\eta_\theta = \int_{\theta_{min}}^{\theta_{max}} p(\theta)cos^2\theta d\theta \quad (3)$$

where $p(\theta)$ is the probability density distribution of θ. A greater η_θ value represents an enhanced fiber alignment in the flexural beams [10].

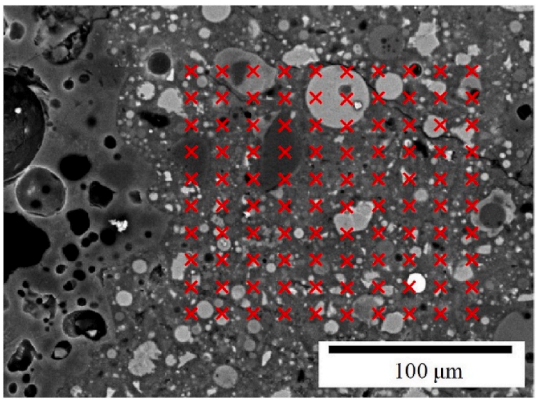

Fig. 3. The 10 × 10 test grid for nano-indentation spots.

2.3.6. Nano-mechanical properties

The Anton Paar Nano-indentation tester was employed to evaluated the nano-mechanical characteristics of C–S–H in surrounding matrix of LWS using a diamond Berkovich tip. The nano-indentation was tested on a 10-mm cube taken from compressive strength sample. The small cube was soaked with epoxy resin followed by polishing of 400-, 600-, and 1200-grit sand papers. The surface of sample was further polished by 9-, 3-, 1-, and 0.25-μm diamond abrasives to enhance the contrast among different phases [41].

Fig. 3 shows the 10 × 10 test grid for nano-indentation spots with a spacing of 15 μm. For each mixture, two 10 × 10 grids (200 spots in total) were measured. The test grids were selected in the regions (around LWS) where little ordinary sand was observed to minimize the influence of sand on test results. For testing of each spot, the load linearly increased at 10 mN/min to 5 mN followed by a 4-s remaining at the maximum load. The load linearly decreased to 0 at a same rate.

2.3.7. Mercury intrusion porosimetry (MIP)

The porosity of non-fibrous UHPC mortar was measured using the IV 9510 MIP with test pressure ranging from 0.28 to 414 MPa. Samples containing LWS were soaked in the isopropyl alcohol to stop cement hydration and were dried at 50 °C for 24 h before testing. In this case, the measured result can represent the total porosity of samples made with LWS that consisted of the porosity of UHPC mortar and LWS.

3. Results and discussion

3.1. Fresh properties

Fig. 4 exhibits the changes in mini-slump flow and rheology of non-

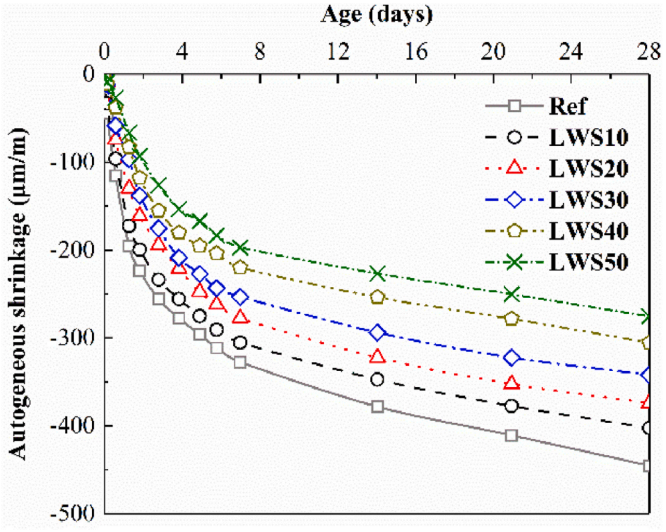

Fig. 5. Autogenous shrinkage of non-fibrous mortar prepared with various LWS contents.

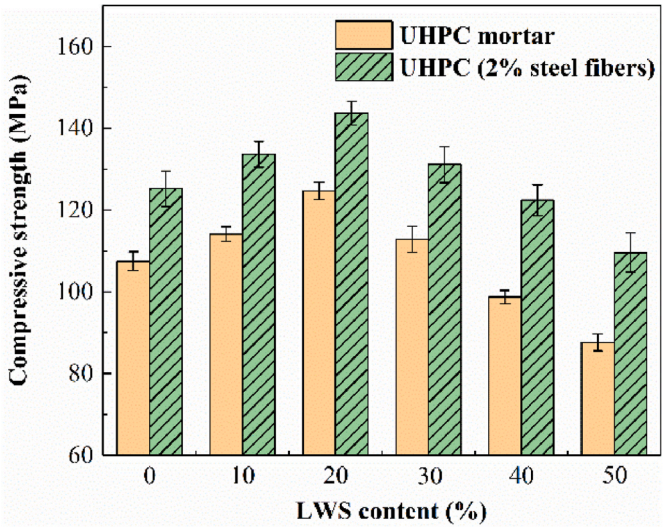

Fig. 6. Changes in compressive strength of UHPCwith LWS contents.

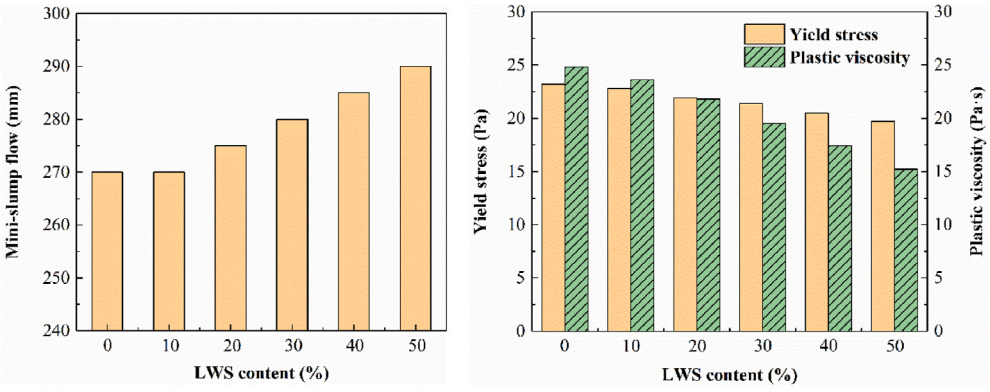

Fig. 4. (a) Mini-slump flow and (b) rheological properties of non-fibrous mortar containing various LWS contents.

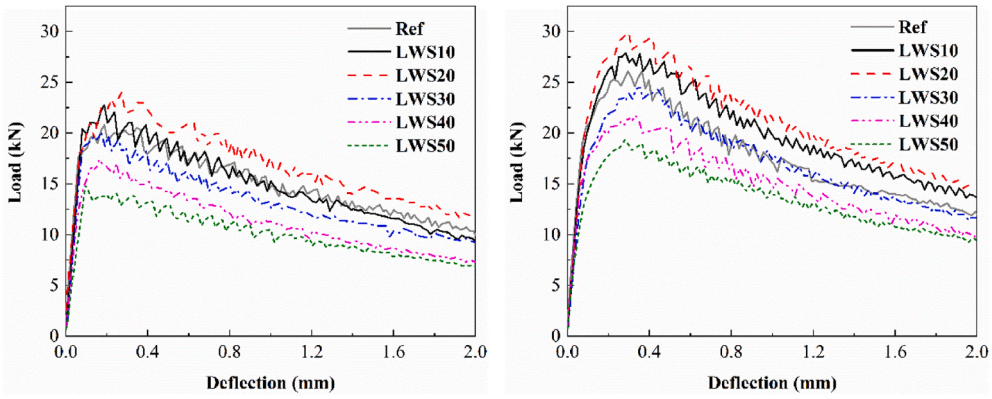

Fig. 7. Flexural load-deflection curves of samples containing various LWS contents: (a) conventional casting method and (b) flow-induced casting method.

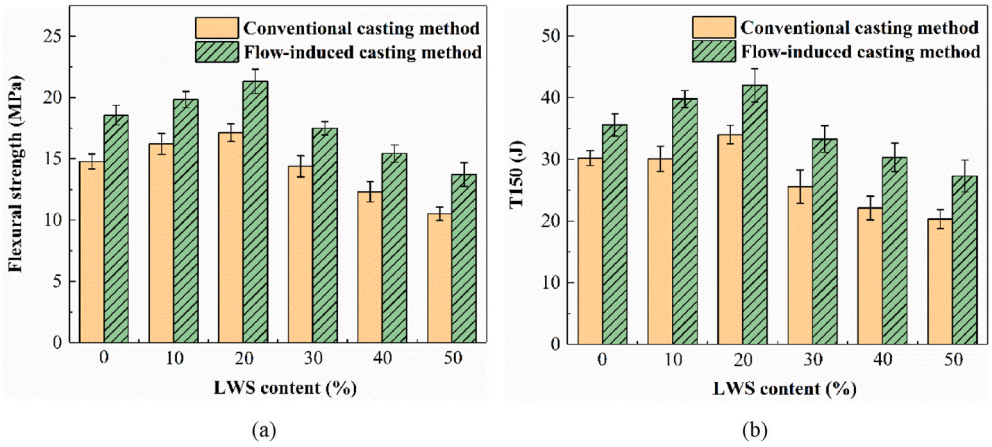

Fig. 8. Changes in (a) flexural strength and (b) T150 of UHPC samples with LWS contents and casting methods.

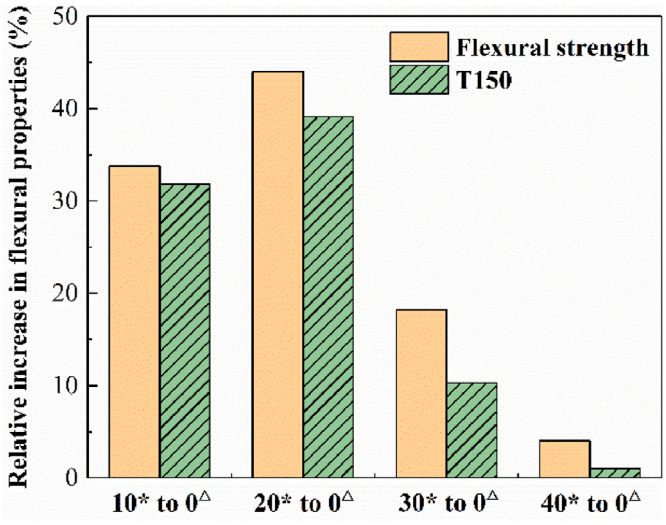

Fig. 9. Relative improvement in flexural strength and T150 of UHPC made by the flow-induced method with addition of various LWS contents relative to those made by the conventional method without any LWS (*: flow-induced casting method, △: conventional casting method).

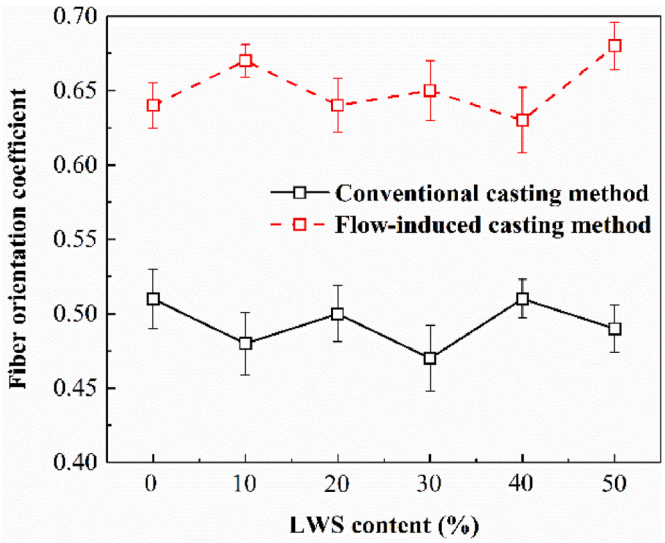

Fig. 10. Fiber orientation coefficients of UHPC prisms prepared with various LWS contents and casting methods.

fibrous mortar with various LWS contents. The mixtures showed self-consolidating performance with mini-slump flow higher than 270 mm. The mini-slump flow increased with the addition of higher LWS content.

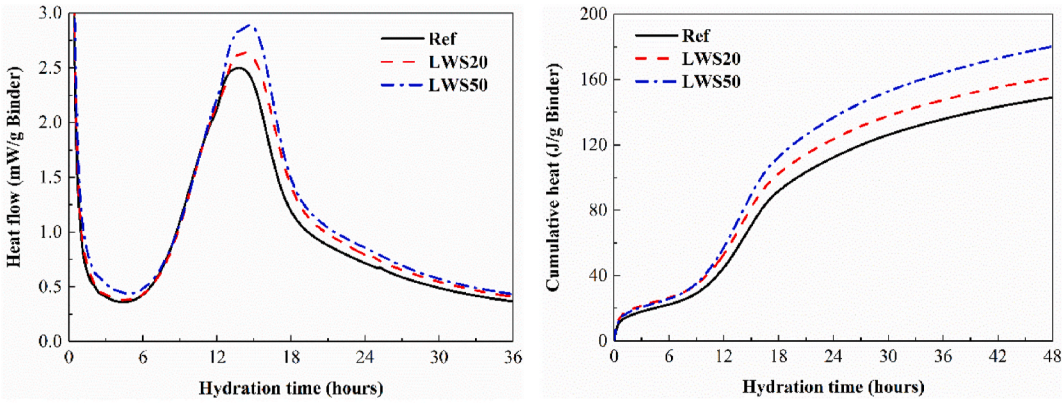

(a) (b)

Fig. 11. (a) Heat flow and (b) cumulative heat of mortar mixtures containing various LWS contents.

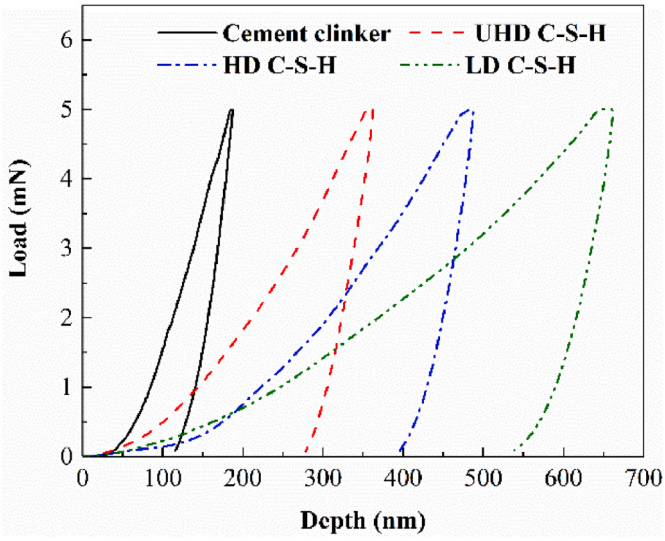

Fig. 12. Load-depth curves of clinker and three types of C–S–H.

As shown in Fig. 4(b), the yield stress and plastic viscosity were reduced by 15% and 40%, respectively, with the increase of LWS content from 0 to 50%. The change in yield stress is in line with the mini-slump flow where the increase in fluidity reduced the yield stress [42,43]. The

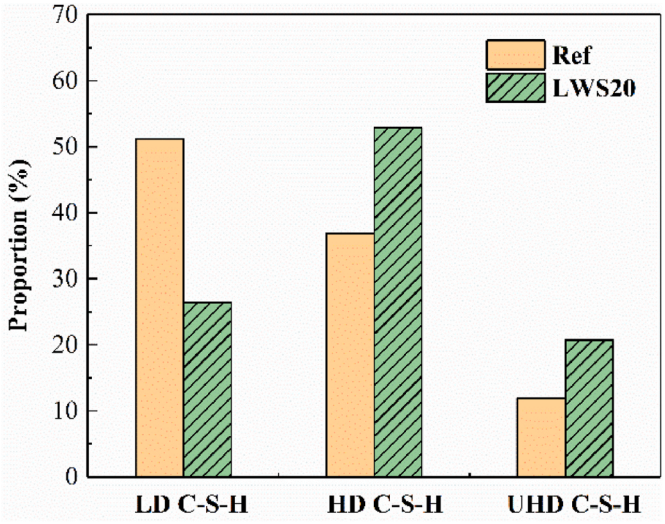

Fig. 14. Percentage of each type of C–S–H for samples made without LWS and with 20% LWS.

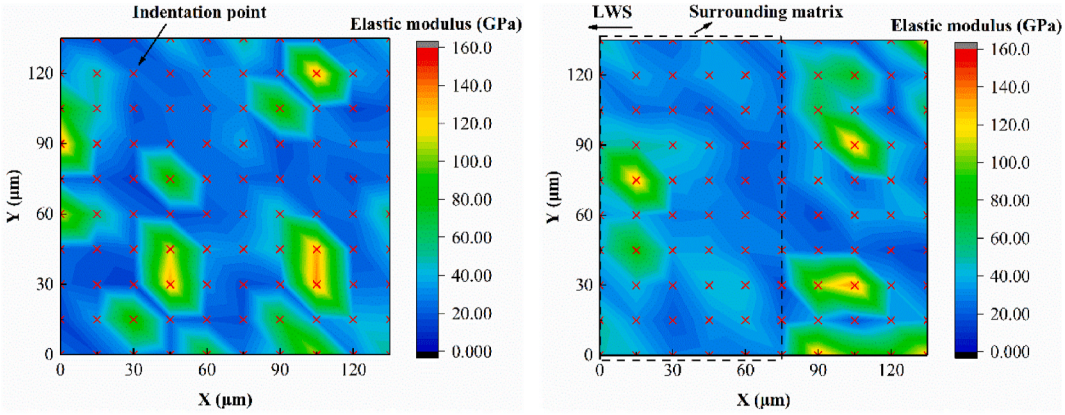

(a) (b)

Fig. 13. Elastic modulus distribution of tested points for samples prepared (a) without LWS and (b) with 20% LWS.

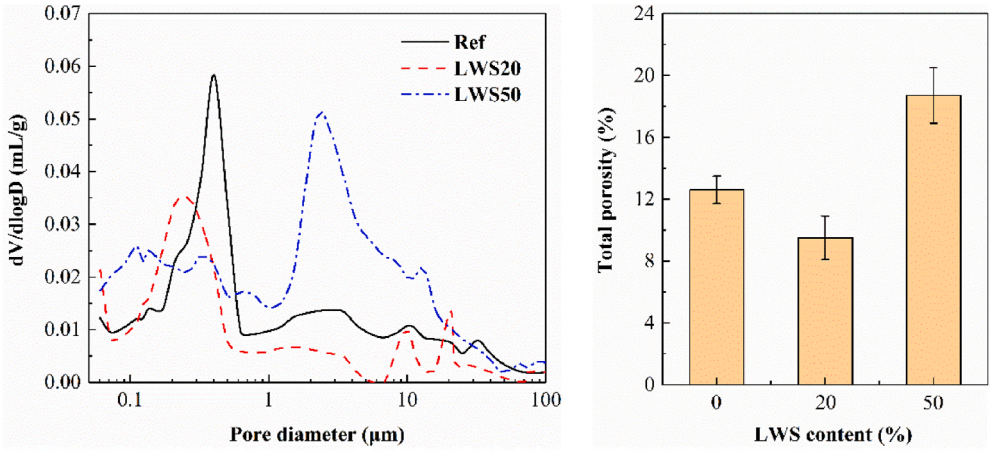

Fig. 15. (a) Pore size distribution and (b) porosity of samples prepared with different LWS contents.

reduction in the rheological parameters with the use of LWS can be due to the lubrication effect of LWS [28].

3.2. Autogenous shrinkage

The evolution of autogenous shrinkage of non-fibrous mortar made with different LWS contents is given in Fig. 5. Overall, the addition of LWS decreased the 28-d autogenous shrinkage. The 28-d autogenous shrinkage was decreased from 450 to 275 μm/m with the increase of LWS content from 0 to 50%. This is due to the water-desorption characteristics of LWS that can delay the reduction of internal humidity with cement hydration [44,45]. Meng and Khayat [33] also reported similar results that the use of 75% LWS in UHPC led to 300 μm/m decrease in 28-d autogenous shrinkage compared to that made without any LWS.

3.3. Compressive strength

The effect of LWS contents on 28-d compressive strength of samples is shown in Fig. 6. The reported results included the strengths tested without and with 2% steel fibers. The use of 20% LWS led to 15% greater compressive strength relative to that prepared without LWS, regardless of the incorporation of steel fibers. This is due to the fact that LWS can offer an internal curing to enhance the cement hydration [29,30]. Such internal curing effect can refine the microstructure of UHPC samples, which is elaborated further in Section 4. However, the increase in LWS content to 50% reduced the compressive strength by approximately 35 MPa for samples made without and with 2% steel fibers.

3.4. Flexural properties

Fig. 7 exhibits the flexural load-deflection curves of UHPC containing various LWS contents. This figure also exhibits the flexural curves of prisms cast by the two casting methods. The curves can be characterized by an elastic ascending zone, a non-linear ascending zone, and a non-linear descending zone [46,47]. In the elastic ascending portion, the flexural load increased linearly with the deflection. In the non-linear ascending portion where fibers can effectively bridge cracks, the flexural load enhanced with the deflection before reaching the peak load. In the non-linear descending zone, the flexural load decreased with the deflection given the pullout of fibers from matrix.

The flexural strength and T150 of samples containing various LWS contents are exhibited in Fig. 8. The flexural strength and T150 were increased as the LWS increasing from 0 to 20%, regardless of the casting method. The use of 20% LWS led to 15% greater flexural strength for UHPC cast using the conventional and flow-induced methods, relative to those made without LWS. Such enhancements for T150 were 10% and 20%, respectively. However, higher LWS content led to the reduction in flexural strength and T150. On the other hand, for a given LWS content, the flow-induced casting method led to 25% and 30% improvements in flexural strength and T150, respectively, relative to UHPC made by the conventional method. This is attributed to the fiber alignment that can increase the crack-bridging ability of fibers [48,49].

The combined use of LWS and fiber alignment can contribute to a coupled effect on improving flexural properties of UHPC. Fig. 9 shows the synergistic effect of LWS and fiber alignment on enhancing flexural strength and T150. Notations “10 to 0”, “20 to 0”, “30 to 0”, and “40 to 0” represent the relative enhancement in flexural properties of UHPC cast by the flow-induced method containing 10%, 20%, 30%, and 40% LWS, respectively, relative to those made by the conventional method without any LWS.

As exhibited in Fig. 9, the flexural strength and T150 can be enhanced by 45% and 40%, respectively, for prismatic samples made with 20% LWS and fiber alignment relative to those of reference mixture with random fiber orientation. Moreover, such synergistic effect can increase the LWS content in UHPC to 40% where the flexural properties are greater than those made without any LWS. This can possibly increase the used content of LWS in UHPC without reduction of mechanical properties.

3.5. Fiber orientation

Fig. 10 shows the changes in fiber orientation coefficients with LWS contents and casting methods. It is shown that the use of LWS had limited effect on fiber orientation. The conventional casting method resulted in an approximately fiber orientation coefficient of 0.5. Such value was increased to approximately 0.65 (30% greater) for the flow-induced casting method. This can enhance the crack-bridging ability of fibers, contributing to the improvement in flexural properties, as elaborated in Section 3.4.

4. Effect of LWS on microstructural and nano-mechanical characteristics

4.1. Hydration kinetics

The heat flow and cumulative heat of mortar mixtures containing various LWS contents is given in Fig. 11. The addition of 50% LWS increased the peak heat flow by 20% relative to that of reference mixture without LWS. Moreover, the time corresponding to the peak heat flow was prolonged by 1 h with the use of 50% LWS compared to that of

reference mixture. Such increase in 48-h cumulative heat was 30% when 50% LWS was added. This indicated the enhanced cement hydration with the addition of LWS.

Despite the enhanced cement hydration of LWS, the addition of 50% LWS can increase the porosity of UHPC according to the MIP results, as shown in Fig. 15. This is due to the excessive introduction of pores of LWS when 50% LWS was added. In this case, the internal curing of LWS can be overwhelmed by the introduction of large pores, leading to the decrease in mechanical properties. Compared to UHPC made without LWS or 20% LWS, the content of pores with diameter greater than 1 μm was significantly increased with the addition of 50% LWS. This is further elaborated in Section 4.3.

4.2. Nano-mechanical properties

The C–S–H in UHPC can be distinguished as three types, including the low density (LD), high density (HD), and ultra-high density (UHD) C–S–H, corresponding to elastic moduli of 10–25, 25–40, and 40–60 GPa, respectively [50–52]. Fig. 12 shows the indentation load-depth curves of clinker, LD, HD, and UHD C–S–H. The greatest depth of C–S–H varied from 300 to 700 nm, depending on the tested type of C–S–H phase. The depth of C–S–H was larger relative to that of clinker given its lower elastic modulus.

Given the load (p), the depth (h), and the greatest indentation depth (h_{max}), the indentation modulus (M) is calculated as following [53]:

$$M = \frac{1}{2}\left(\frac{dp}{dh}\sqrt{\frac{\pi}{A}}\right)_{h=h_{max}} \tag{4}$$

where A (μm^2) is the projected contact area that is achieved using the Oliver and Pharr's method [54].

Given the Poisson's ratio of analyzed phase (v), the elastic modulus (E_1) and the Poisson's ratio (v_1) of tester tip, the elastic modulus (E) can be calculated by Eq. (5):

$$\frac{1}{M} = \frac{1-v^2}{E} + \frac{1-v_1^2}{E_1} \tag{5}$$

Fig. 13 shows the elastic modulus of tested points for samples prepared without LWS and with 20% LWS. The first column of 10 × 10 test grid is set as X = 0 μm. For samples prepared without LWS, the test grid was selected randomly. For samples made with 20% LWS, the first column (X = 0 μm) was selected near the LWS particle to evaluate the influence of LWS on C–S–H elastic modulus in surrounding matrix. The blue, light blue, and light green areas correspond to the LD (10–25 GPa), HD (25–40 GPa), UHD C–S–H (40–60 GPa), respectively. The green, yellow, and orange areas correspond to elastic modulus greater than 60 GPa, representing the un-hydrated clinker.

The use of 20% LWS was shown to decrease the proportions of un-hydrated clinker and LD C–S–H, and increase the proportions of HD and UHD C–S–H. The width of surrounding matrix can vary with the changes in absorption and desorption characteristics as well as the pretreatment method of LWS [29,44]. In the case of this study, the width of surrounding matrix can be on the order of 75 μm, as demonstrated in Fig. 13(b). In the surrounding matrix, the percentages of HD and UHD C–S–H were significantly greater than un-hydrated clinker and LD C–S–H. This reflected that the internal curing effect of LWS indeed enhanced cement hydration and C–S–H formation in surrounding matrix. This is in well agreement with the hydration kinetics results where the use of 20% LWS led to a greater heat flow and cumulative heat due to the enhanced cement hydration with the addition of LWS.

The percentages of each type of C–S–H of mixtures made without LWS and with 20% LWS are shown in Fig. 14. For samples made without LWS, the proportions of these three C–S–H were 51%, 37%, and 12%, respectively. The proportions of the latter two types of C–S–H were increased to 53% and 21%, respectively, with the use of 20% LWS. Such increased HD and UHD C–S–H percentages can therefore contribute to greater mechanical properties of UHPC.

4.3. Pore structure

Fig. 15 shows the 28-d pore size distribution and porosity results of Ref, LWS20, and LWS50 samples. This figure reports the average results of three tests for each mixture to enhance the accuracy. The most probable diameter refers to the pore size corresponding to the highest peak of the curve. As shown in Fig. 15(a), the most probable diameter decreased with the use of 20% LWS, relative to that without any LWS. This led to the reduction of 28-d porosity from 12.5% to 9.5%. Given the internal curing effect, the pre-saturated LWS can release water during curing of samples to secure a greater cement hydration degree [29,30]. As concluded from Section 4.2, the use of 20% LWS can enhance the proportion of HD and UHD C–S–H, leading to a denser degree of matrix. Moreover, the hydration products can fill portion of the pores introduced by LWS when the LWS was used at 20% [33]. This led to the refinement in microstructure of UHPC.

However, the most probable diameter and porosity significantly increased with the further increase in LWS content. The porosity increased to 19% when 50% LWS was added. This was also found in Ref. [33] where the enhancement of LWS content from 25% to 50% resulted in 110% greater porosity. This is attributed to the excessive use of LWS, which can introduce more large pores. As shown in Fig. 15(a), the content of pores with diameter greater than 1 μm was significantly increased with the use of 50% LWS, leading to the increased porosity of UHPC. This resulted in the reduction in mechanical properties, despite of the enhanced cement hydration (Section 4.1) [44]. Therefore, it can be concluded that the use of 20% LWS can result in a maximum net effect in improving the microstructure and increasing the mechanical properties of UHPC.

5. Conclusions

In this paper, the influence of pre-saturated lightweight sand (LWS) on the mechanical and microstructural characteristics of UHPC prismatic samples with the alignment of fibers was studied. The synergistic effect of LWS and predominant fiber alignment on mechanical properties was evaluated. The investigated volume of LWS ranged from 0 to 50%. On the basis of experimental results, the following conclusions can be obtained:

1. The 28-d autogenous shrinkage was decreased from 450 to 275 μm/m with the increase of LWS content from 0 to 50%.
2. The addition of 20% LWS can result in the maximum improvements of 15%, 15%, and 20% in compressive strength, flexural strength, and dissipated energy (T150), respectively, relative to UHPC made without LWS.
3. The combination of 20% LWS and fiber alignment resulted in the synergistic enhancement of 45% and 40% in flexural strength and T150, respectively, relative to UHPC without any LWS and having random fiber orientation.
4. The use of LWS enhanced the cement hydration. The proportion of HD and UHD C–S–H in surrounding matrix of LWS was increased from 50% to 75% with the use of 20% LWS.
5. The 28-d porosity was reduced from 12.5% to 9.5% with the addition of 20% LWS due to the internal curing of LWS. However, such internal curing can be overwhelmed by the introduced pores of LWS when 50% LWS was used, leading to significant increase in porosity.

Declaration of competing interest

The authors declare that they have no known competing financial interests or personal relationships that could have appeared to influence the work reported in this paper.

Acknowledgment

This work was carried out at the Clayco Advanced Construction and Material Laboratory (ACML) of the Center for Infrastructure Engineering Studies (CIES) at Missouri S&T and was supported by the National Natural Science Foundation of China (grant number: U2106220).

References

[1] F. de Larrard, T. Sedran, Optimization of ultra-high-performance concrete by the use of a packing model, Cement Concr. Res. 24 (1994) 997–1009, https://doi.org/10.1016/0008-8846(94)90022-1.
[2] K. Habel, M. Viviani, E. Denarié, E. Brühwiler, Development of the mechanical properties of an ultra-high performance fiber reinforced concrete (UHPFRC), Cement Concr. Res. 36 (2006) 1362–1370, https://doi.org/10.1016/j.cemconres.2006.03.009.
[3] K.H. Khayat, W. Meng, K. Vallurupalli, L. Teng, Rheological properties of ultra-high-performance concrete — an overview, Cement Concr. Res. 124 (2019) 105828, https://doi.org/10.1016/j.cemconres.2019.105828.
[4] B. Graybeal, E. Brühwiler, B.-S. Kim, F. Toutlemonde, Y.L. Voo, A. Zaghi, International perspective on UHPC in bridge engineering, J. Bridge Eng. 25 (2020), 04020094, https://doi.org/10.1061/(asce)be.1943-5592.0001630.
[5] Z.B. Haber, B.A. Graybeal, Performance of Grouted Connections for Prefabricated Bridge Deck Elements, 2018.
[6] P. Richard, M. Cheyrezy, Composition of reactive powder concretes, Cement Concr. Res. 25 (1995) 1501–1511, https://doi.org/10.1016/0008-8846(95)00144-2.
[7] R. Yu, P. Spiesz, H.J.H. Brouwers, Mix design and properties assessment of ultra-high performance fibre reinforced concrete (UHPFRC), Cement Concr. Res. 56 (2014) 29–39, https://doi.org/10.1016/j.cemconres.2013.11.002.
[8] X. Wang, R. Yu, Q. Song, Z. Shui, Z. Liu, S. Wu, D. Hou, Optimized design of ultra-high performance concrete (UHPC) with a high wet packing density, Cement Concr. Res. 126 (2019) 105921, https://doi.org/10.1016/j.cemconres.2019.105921.
[9] N. Banthia, M. Sappakittipakorn, Toughness enhancement in steel fiber reinforced concrete through fiber hybridization, Cement Concr. Res. 37 (2007) 1366–1372, https://doi.org/10.1016/j.cemconres.2007.05.005.
[10] H. Huang, X. Gao, L. Teng, Fiber alignment and its effect on mechanical properties of UHPC: an overview, Construct. Build. Mater. 296 (2021) 123741, https://doi.org/10.1016/j.conbuildmat.2021.123741.
[11] L. Teng, W. Meng, K.H. Khayat, Rheology control of ultra-high-performance concrete made with different fiber contents, Cement Concr. Res. 138 (2020) 106222, https://doi.org/10.1016/j.cemconres.2020.106222.
[12] Q. Song, R. Yu, Z. Shui, X. Wang, S. Rao, Z. Lin, Z. Wang, Key parameters in optimizing fibres orientation and distribution for ultra-high performance fibre reinforced concrete (UHPFRC), Construct. Build. Mater. 188 (2018) 17–27, https://doi.org/10.1016/j.conbuildmat.2018.08.102.
[13] L. Teng, H. Huang, J. Du, K.H. Khayat, Prediction of fiber orientation and flexural performance of UHPC based on suspending mortar rheology and casting method, Cement Concr. Compos. 122 (2021) 104142, https://doi.org/10.1016/j.cemconcomp.2021.104142.
[14] D.-Y. Yoo, G. Zi, S.-T. Kang, Y.-S. Yoon, Biaxial flexural behavior of ultra-high-performance fiber-reinforced concrete with different fiber lengths and placement methods, Cement Concr. Compos. 63 (2015) 51–66.
[15] S.T. Kang, J.K. Kim, Numerical simulation of the variation of fiber orientation distribution during flow molding of ultra high performance cementitious composites (UHPCC), Cement Concr. Compos. 34 (2012) 208–217, https://doi.org/10.1016/j.cemconcomp.2011.09.015.
[16] Z. Ge, A.M. Tawfek, H. Zhang, Y. Yang, H. Yuan, R. Sun, Z. Wang, Influence of an extrusion approach on the fiber orientation and mechanical properties of engineering cementitious composite, Construct. Build. Mater. 306 (2021) 124876, https://doi.org/10.1016/j.conbuildmat.2021.124876.
[17] J. Liu, X. Ma, C. Shi, S. Drissi, Internal curing of blended cement pastes with ultra-low water-to-cement ratio: absorption/desorption kinetics of superabsorbent polymer, J. Am. Ceram. Soc. 104 (2021) 3603–3618, https://doi.org/10.1111/jace.17730.
[18] J. Liu, N. Farzadnia, K.H. Khayat, C. Shi, Effects of SAP characteristics on internal curing of UHPC matrix, Construct. Build. Mater. 280 (2021) 122530, https://doi.org/10.1016/j.conbuildmat.2021.122530.
[19] D. Cusson, T. Hoogeveen, An experimental approach for the analysis of early-age behaviour of high-performance concrete structures under restrained shrinkage, Cement Concr. Res. 37 (2007) 200–209, https://doi.org/10.1016/j.cemconres.2006.11.005.
[20] L. Teng, M. Valipour, K.H. Khayat, Design and performance of low shrinkage UHPC for thin bonded bridge deck overlay, Cement Concr. Compos. 118 (2021) 103953, https://doi.org/10.1016/j.cemconcomp.2021.103953.
[21] M. Valipour, K.H. Khayat, Coupled effect of shrinkage-mitigating admixtures and saturated lightweight sand on shrinkage of UHPC for overlay applications, Construct. Build. Mater. 184 (2018) 320–329, https://doi.org/10.1016/j.conbuildmat.2018.06.191.
[22] J. Liu, N. Farzadnia, C. Shi, X. Ma, Shrinkage and strength development of UHSC incorporating a hybrid system of SAP and SRA, Cement Concr. Compos. 97 (2019) 175–189, https://doi.org/10.1016/j.cemconcomp.2018.12.029.
[23] L. Yang, C. Shi, Z. Wu, Mitigation techniques for autogenous shrinkage of ultra-high-performance concrete – a review, Compos. B Eng. 178 (2019) 107456, https://doi.org/10.1016/j.compositesb.2019.107456.
[24] J. Justs, M. Wyrzykowski, D. Bajare, P. Lura, Internal curing by superabsorbent polymers in ultra-high performance concrete, Cement Concr. Res. 76 (2015) 82–90, https://doi.org/10.1016/j.cemconres.2015.05.005.
[25] D. Cusson, T. Hoogeveen, Internal curing of high-performance concrete with pre-soaked fine lightweight aggregate for prevention of autogenous shrinkage cracking, Cement Concr. Res. 38 (2008) 757–765, https://doi.org/10.1016/j.cemconres.2008.02.001.
[26] Y. Sun, R. Yu, Z. Shui, X. Wang, D. Qian, B. Rao, J. Huang, Y. He, Understanding the porous aggregates carrier effect on reducing autogenous shrinkage of Ultra-High Performance Concrete (UHPC) based on response surface method, Construct. Build. Mater. 222 (2019) 130–141, https://doi.org/10.1016/j.conbuildmat.2019.06.151.
[27] K. Liu, R. Yu, Z. Shui, X. Li, C. Guo, B. Yu, S. Wu, Optimization of autogenous shrinkage and microstructure for Ultra-High Performance Concrete (UHPC) based on appropriate application of porous pumice, Construct. Build. Mater. 214 (2019) 369–381, https://doi.org/10.1016/j.conbuildmat.2019.04.089.
[28] K. Liu, R. Yu, Z. Shui, S. Yi, X. Li, G. Ling, Y. He, Influence of external water introduced by coral sand on autogenous shrinkage and microstructure development of Ultra-High Strength Concrete (UHSC), Construct. Build. Mater. 252 (2020) 119111, https://doi.org/10.1016/j.conbuildmat.2020.119111.
[29] X. Ma, J. Liu, C. Shi, A review on the use of LWA as an internal curing agent of high performance cement-based materials, Construct. Build. Mater. 218 (2019) 385–393, https://doi.org/10.1016/j.conbuildmat.2019.05.126.
[30] P. Shen, L. Lu, F. Wang, Y. He, S. Hu, J. Lu, H. Zheng, Water desorption characteristics of saturated lightweight fine aggregate in ultra-high performance concrete, Cement Concr. Compos. 106 (2020) 103456, https://doi.org/10.1016/j.cemconcomp.2019.103456.
[31] T. Lu, Z. Li, H. Huang, Restraining effect of aggregates on autogenous shrinkage in cement mortar and concrete, Construct. Build. Mater. 289 (2021) 123166, https://doi.org/10.1016/j.conbuildmat.2021.123166.
[32] D.-Y. Yoo, N. Banthia, Mechanical properties of ultra-high-performance fiber-reinforced concrete: a review, Cement Concr. Compos. 73 (2016) 267–280, https://doi.org/10.1016/j.cemconcomp.2016.08.001.
[33] W. Meng, K. Khayat, Effects of saturated lightweight sand content on key characteristics of ultra-high-performance concrete, Cement Concr. Res. 101 (2017) 46–54, https://doi.org/10.1016/j.cemconres.2017.08.018.
[34] Y. Liu, Y. Wei, Effect of calcined bauxite powder or aggregate on the shrinkage properties of UHPC, Cement Concr. Compos. 118 (2021) 103967, https://doi.org/10.1016/j.cemconcomp.2021.103967.
[35] Y. Liu, Y. Wei, Internal curing efficiency and key properties of UHPC influenced by dry or prewetted calcined bauxite aggregate with different particle size, Construct. Build. Mater. 312 (2021) 125406, https://doi.org/10.1016/j.conbuildmat.2021.125406.
[36] W. Meng, M. Valipour, K.H. Khayat, Optimization and performance of cost-effective ultra-high performance concrete, Mater. Struct. 50 (2016) 29, https://doi.org/10.1617/s11527-016-0896-3.
[37] H. Huang, X. Gao, L. Li, H. Wang, Improvement effect of steel fiber orientation control on mechanical performance of UHPC, Construct. Build. Mater. 188 (2018), https://doi.org/10.1016/j.conbuildmat.2018.08.146.
[38] H. Huang, X. Gao, A. Zhang, Numerical simulation and visualization of motion and orientation of steel fibers in UHPC under controlling flow condition, Construct. Build. Mater. 199 (2019) 624–636, https://doi.org/10.1016/j.conbuildmat.2018.12.055.
[39] J. Liu, N. Farzadnia, C. Shi, Effects of superabsorbent polymer on interfacial transition zone and mechanical properties of ultra-high performance concrete, Construct. Build. Mater. 231 (2020) 117142, https://doi.org/10.1016/j.conbuildmat.2019.117142.
[40] D.-Y. Yoo, N. Banthia, Y.-S. Yoon, Predicting the flexural behavior of ultra-high-performance fiber-reinforced concrete, Cement Concr. Compos. 74 (2016) 71–87, https://doi.org/10.1016/j.cemconcomp.2016.09.005.
[41] G. Constantinides, F.-J. Ulm, The effect of two types of C-S-H on the elasticity of cement-based materials: results from nanoindentation and micromechanical modeling, Cement Concr. Res. 34 (2004) 67–80, https://doi.org/10.1016/S0008-8846(03)00230-8.
[42] N. Roussel, Correlation between yield stress and slump: comparison between numerical simulations and concrete rheometers results, Mater. Struct. 39 (2006) 501–509.
[43] L. Teng, J. Zhu, K.H. Khayat, J. Liu, Effect of welan gum and nanoclay on thixotropy of UHPC, Cement Concr. Res. 138 (2020) 106238, https://doi.org/10.1016/j.cemconres.2020.106238.
[44] J. Liu, C. Shi, N. Farzadnia, X. Ma, Effects of pretreated fine lightweight aggregate on shrinkage and pore structure of ultra-high strength concrete, Construct. Build. Mater. 204 (2019) 276–287, https://doi.org/10.1016/j.conbuildmat.2019.01.205.
[45] P. Shen, J.-X. Lu, L. Lu, Y. He, F. Wang, S. Hu, An alternative method for performance improvement of ultra-high performance concrete by internal curing: role of physicochemical properties of saturated lightweight fine aggregate, Construct. Build. Mater. 312 (2021) 125373, https://doi.org/10.1016/j.conbuildmat.2021.125373.
[46] W. Meng, K.H. Khayat, Mechanical properties of ultra-high-performance concrete enhanced with graphite nanoplatelets and carbon nanofibers, Compos. B Eng. 107 (2016) 113–122, https://doi.org/10.1016/j.compositesb.2016.09.069.

[47] W. Meng, K.H. Khayat, Improving flexural performance of ultra-high-performance concrete by rheology control of suspending mortar, Compos. B Eng. 117 (2017) 26–34.
[48] H. Huang, X. Gao, K.H. Khayat, Contribution of fiber alignment on flexural properties of UHPC and prediction using the Composite Theory, Cement Concr. Compos. 118 (2021) 103971, https://doi.org/10.1016/j.cemconcomp.2021.103971.
[49] H. Huang, X. Gao, K.H. Khayat, Contribution of fiber orientation to enhancing dynamic properties of UHPC under impact loading, Cement Concr. Compos. 121 (2021) 104108, https://doi.org/10.1016/j.cemconcomp.2021.104108.
[50] P. Mondal, S.P. Shah, L. Marks, A reliable technique to determine the local mechanical properties at the nanoscale for cementitious materials, Cement Concr. Res. 37 (2007) 1440–1444, https://doi.org/10.1016/j.cemconres.2007.07.001.
[51] P. Shen, L. Lu, Y. He, F. Wang, S. Hu, The effect of curing regimes on the mechanical properties, nano-mechanical properties and microstructure of ultra-high performance concrete, Cement Concr. Res. 118 (2019) 1–13, https://doi.org/10.1016/j.cemconres.2019.01.004.
[52] H. Huang, L. Teng, X. Gao, K.H. Khayat, F. Wang, Z. Liu, Effect of carbon nanotube and graphite nanoplatelet on composition, structure, and nano-mechanical properties of C-S-H in UHPC, Cem, Concr. Res. 154 (2022) 106713, https://doi.org/10.1016/j.cemconres.2022.106713.
[53] L. Sorelli, G. Constantinides, F.J. Ulm, F. Toutlemonde, The nano-mechanical signature of Ultra High Performance Concrete by statistical nanoindentation techniques, Cement Concr. Res. 38 (2008) 1447–1456, https://doi.org/10.1016/j.cemconres.2008.09.002.
[54] W.C. Oliver, G.M. Pharr, An improved technique for determining hardness and elastic modulus using load and displacement sensing indentation experiments, J. Mater. Res. 7 (1992) 1564–1583, https://doi.org/10.1557/JMR.1992.1564.